Research Article Vol. 59, No. 21 / 20 July 2020 / Applied Optics 6347

applied optics

Model of a tunable hybrid Tamm mode–liquid crystal device

Maxim V. Pyatnov,[1,2,*] Rashid G. Bikbaev,[1,2] Ivan V. Timofeev,[1,2] and Stepan Ya. Vetrov[1,2]

[1]Kirensky Institute of Physics, Federal Research Center "Krasnoyarsk Scientific Center, Russian Academy of Sciences, Siberian Branch", Krasnoyarsk, Russia
[2]Siberian Federal University, Krasnoyarsk, Russia
*Corresponding author: MaksPyatnov@yandex.ru

Received 22 April 2020; revised 18 June 2020; accepted 20 June 2020; posted 22 June 2020 (Doc. ID 395901); published 16 July 2020

A concept of an easily tunable device based on hybrid Tamm modes is proposed. The device can be controlled using a high-sensitivity chiral liquid crystal serving as a mirror. The coupling of the chiral optical Tamm state with the Tamm plasmons is predicted. The Tamm plasmons are excited at different frequencies for the orthogonal linear polarizations, while the chiral Tamm state is excited at only one frequency. The properties of the proposed model are analytically and numerically calculated. The possibility of creating a two- and three-mode laser with tunable characteristics on the basis of the proposed model is discussed.

https://doi.org/10.1364/AO.395901

1. INTRODUCTION

The Tamm modes, including Tamm plasmons (Tamm plasmon polaritons) and optical Tamm states, have been intensively studied for more than a decade [1–3]. The interest in these modes is due to their potential for application in lasers [4], emitters [5,6], absorbers [7,8], and sensors [9] as well as photovoltaic [10], topological photonic [11,12], and other devices [13–16].

The Tamm modes can be strongly coupled with each other or with resonances of a different nature, e.g., the cavity modes, exciton polaritons, and surface plasmons [17–22]. Such hybrid modes are characterized by avoided crossing of two resonances at the detuning of the position of one of the resonances, which is widely used in sensors [23,24].

Liquid crystals are promising for wavelength-tunable Tamm plasmons [14,25–27]. They can be used both as service components for changing the optical properties and as Bragg reflectors. In the latter case, as a rule, cholesteric liquid crystals (CLCs) are used. In contrast to scalar dielectric multilayers, CLCs have the only band gap at the normal incidence, which exists exclusively for the circular polarization of light co-handed with the cholesteric helix twist [28].

In contrast to the case of metals or conventional dielectric materials, the circularly polarized radiation reflected from a CLC preserves its polarization direction. Therefore, it is difficult to observe the Tamm modes localized between a CLC and a metallic layer [13,29,30]. A possible tool for observing them is a polarization-preserving (handedness-preserving or chiral) anisotropic mirror (PPAM) [31–33].

Here we discuss the design of a device based on hybrid Tamm modes. The proposed structure supports the Tamm modes of two types: the Tamm plasmon (TP) and the chiral optical Tamm state (COTS). It is proposed to tune the COTS spectral position by changing the parameters that are only inherent in a chiral medium, such as a CLC.

2. DESIGN OF THE DEVICE

Figure 1 shows a design of the proposed device. A multilayer anisotropic mirror is bounded by a metallic film on one side and by a cholesteric layer on the other. The mirror is a structure that preserves the polarization of the incident light. It consists of N periods of alternating uniaxial dielectric layers with refractive indices n_e^m and n_o^m. Thus, each PPAM layer is anisotropic with n_e^m and n_o^m. Herewith, each layer is rotated relative to the previous one by 90°. The PPAM period thickness is $2a$. A cholesteric is characterized by extraordinary and ordinary refractive indices n_e and n_o and helix pitch p. The angle between the CLC director and the optical axis of the PPAM layer adjacent to it is designated by φ. The PPAM layer adjacent to the metallic film with thickness d_m was assumed to have different thickness d. The structure is surrounded by a medium with the refractive index equal to the averaged CLC refractive index $n_{\text{ext}} = (n_e + n_o)/2$. Such an approach makes it possible to weaken the effect of Fresnel reflection on the spectral properties of the sample.

The two Tamm modes that can be excited in the proposed structure are the TP localized at the metal–mirror interface and

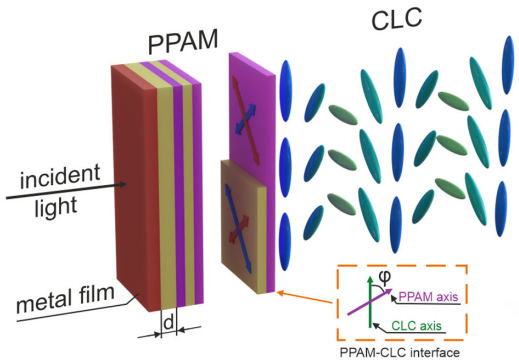

Fig. 1. Schematic of the structure consisting of a metal film, a polarization-preserving anisotropic mirror (PPAM), and a cholesteric liquid crystal (CLC). Color arrows show the directions of the optical axes of the PPAM layers.

the COTS localized at the PPAM–cholesteric interface. It is expected that the change in the parameters of the mirror allows us to tune the coupling between the modes.

At the interface between the metallic film and the multilayer Bragg reflector, the role of which in the investigated model is played by the PPAM, a TP can be excited. The TP frequency is determined from the condition [3]

$$r_{\mathrm{Me}} r_{\mathrm{PPAM}} e^{2i\chi} = 1, \tag{1}$$

where r_{Me} and r_{PPAM} are the amplitude reflectivities of the metallic and PPAM layers, and $\chi = n_a d\omega/c$ is the phase variation in the wave with frequency ω propagating in the boundary layer with thickness d and refractive index n_a.

The amplitude reflectivity of a multilayer consisting of N periods is determined using the equation [34]

$$r_{\mathrm{PPAM}} = \frac{CU_{N-1}}{AU_{N-1} - U_{N-2}}. \tag{2}$$

In Eq. (2), $U_N = \frac{\sin 2a(N+1)K}{\sin 2aK}$, and $K = \frac{1}{2a}\arccos(\frac{A+D}{2})$ is the Bloch wavenumber.

Since we only analyze the case of normal incidence, the elements A, B, C, and D of the transfer matrix for one cell, which relate the amplitudes of plane waves in the first layer of the unit cell to the amplitudes in the neighboring unit cell, can be written as

$$A = e^{ik_{1z}a}\left[\cos k_{2z}a + \frac{1}{2}i\left(\frac{k_{2z}}{k_{1z}} + \frac{k_{1z}}{k_{2z}}\right)\sin k_{2z}a\right],$$

$$B = e^{-ik_{1z}a}\left[\frac{1}{2}i\left(\frac{k_{2z}}{k_{1z}} - \frac{k_{1z}}{k_{2z}}\right)\sin k_{2z}a\right],$$

$$C = e^{ik_{1z}a}\left[-\frac{1}{2}i\left(\frac{k_{2z}}{k_{1z}} - \frac{k_{1z}}{k_{2z}}\right)\sin k_{2z}a\right],$$

$$D = e^{-ik_{1z}a}\left[\cos k_{2z}a - \frac{1}{2}i\left(\frac{k_{2z}}{k_{1z}} + \frac{k_{1z}}{k_{2z}}\right)\sin k_{2z}a\right], \tag{3}$$

where $k_{1z} = (\omega/c)n_e^{m^2}$ and $k_{2z} = (\omega/c)n_o^{m^2}$ are the wave vectors for the first and second media, respectively.

The amplitude reflectivity r_{Me} of the metallic layer can be determined using the Airy formula [35]:

$$r_{\mathrm{Me}} = \frac{r_{12} + r_{23}e^{4\pi d_m \omega n_m/c}}{1 + r_{12}r_{23}e^{4\pi d_m \omega n_m/c}}. \tag{4}$$

In Eq. (4), $r_{12} = \frac{n_{\mathrm{ext}} - n_m}{n_{\mathrm{ext}} + n_m}$ and $r_{23} = \frac{n_m - n_a}{n_m + n_a}$. Here, n_a is the refractive index of the layer adjacent to the metal, and d_m and n_m are the thickness and refractive index of the metal, respectively, which is expressed, in the Drude approximation, by the formula

$$n_m^2 = \epsilon_0 - \frac{\omega_p^2}{\omega(\omega + i\gamma)}, \tag{5}$$

where ϵ_0 is the contribution of the ionic subsystem, ω_p is the plasma frequency, and γ is the reciprocal relaxation time.

Near the Bragg frequency of the mirror, the amplitudes r_{PPAM} and r_{Me} are almost unity. We designate the phases of the waves reflected from the PPAM and metal by φ_{PPAM} and φ_{Me}, respectively, and write Eq. (1) in the form

$$\pi m = \varphi_{\mathrm{PPAM}} + \varphi_{\mathrm{Me}} + 2\chi, \tag{6}$$

where m is an arbitrary integer.

A feature of the investigated model is that, at the interface between the metal and the PPAM, the TP is excited at different frequencies for the orthogonal linear polarizations of the incident light.

The frequency of the COTS localized at the interface between two media with reflectivities r_{PPAM} and r_{CLC} and the angle between the CLC director and optical axis of the last anisotropic layer adjacent to the CLC φ can be found similarly from the equation [33]

$$r_{\mathrm{PPAM}} r_{\mathrm{CLC}} e^{2i\varphi} = 1. \tag{7}$$

The amplitude reflectivity of a cholesteric is [28]

$$r_{\mathrm{CLC}} = \frac{i\delta \sin qd}{((q\tau/\kappa^2)\cos qd + i((\tau/2\kappa)^2 + (q/\kappa)^2 - 1)\sin qd}. \tag{8}$$

Here $\delta = \frac{(n_e^2 - n_0^2)}{(n_e^2 + n_0^2)}$, $\kappa = \frac{\omega\sqrt{((n_e^2 + n_0^2)/2)}}{c}$, and $\tau = \frac{4\pi}{p}$ is the CLC reciprocal lattice vector. The wave vector of the mode diffracting in the CLC, which has a band gap, is

$$q = \kappa\sqrt{1 + (\tau/2\kappa)^2 - \sqrt{(\tau/\kappa)^2 + \delta^2}}. \tag{9}$$

Near the Bragg frequency, the amplitudes r_{PPAM} and r_{CLC} are almost unity. We designate the phases of the waves reflected from the PPAM and CLC by φ_{PPAM} and φ_{CLC} and write Eq. (7) in the form

$$\pi m = \varphi_{\mathrm{PPAM}} + \varphi_{\mathrm{CLC}} + 2\varphi. \tag{10}$$

Thus, in the proposed structure (Fig. 1), the frequencies of certain excited resonances are determined using Eqs. (6) or (10). The two modes are localized at different PPAM boundaries. It is expected that, at small PPAM thickness, the electromagnetic field profiles of the localized modes are spatially overlapped. When mode frequencies coincide, the coupling between the resonances leads to their splitting.

We mainly consider the case of the normal incidence of circularly polarized light onto the structure. This is due to the fact that the cholesteric eigenmode has quasi-circular polarization [28]. In addition, the circular polarization can always be presented as a sum of orthogonal linear polarizations.

3. RESULTS

A. Tamm Plasmons

First, we discuss the features of the excitation of pure TPs in the proposed model (Fig. 1). For this purpose, we consider the model without a CLC. The TP position is conventionally tuned by changing thickness d or refractive index n_a of the layer adjacent to the metallic film. For the light of each of the linear polarizations propagating along the PPAM optical axes, the PPAM is an anisotropic photonic crystal; therefore, at the orthogonal linear polarizations of the incident light, the TPs are excited at different wavelengths. Figure 2 shows the transmittance spectrum for a pure TP structure without cholesteric versus the thickness d of the layer adjacent to the metallic film. The calculation was made using the Berreman matrix method [36]. For the light propagating along the z axis of the cholesteric helix with frequency ω, the equation is $\partial\psi/\partial z = (-i\omega/c)\Delta\psi$, where $\psi(z) = (E_x, H_y, E_y, -H_x)^T$, and $\Delta(z)$ is the Berreman matrix, which depends on the permittivity and incident wave vector. For Berreman method implementation, we use a self-made program verified by Lumerical commercial package calculations. In the simulation, we used PPAM refractive indices of $n_e^m = 1.71$ and $n_o^m = 1.54$, a period of $2a = 200$ nm, and a number of periods of $N = 20$. The metallic film thickness was taken to be $d_m = 50$ nm, and the other film parameters were $\epsilon_0 = 5$, $\hbar\omega_p = 9$ eV, and $\hbar\gamma = 0.02$ eV, which are typical of silver.

The white and red lines in Fig. 2 show the TP wavelengths for the TM and TE polarizations of the incident light calculated using Eq. (6). By TM and TE polarizations of incident light, we mean orthogonal linear polarizations directed along the optical axes of the first PPAM layer with refractive indices n_e^m and n_o^m, respectively. At the parameters used, the PPAM band gap center is located at a wavelength of 650 nm. At $d = 184$ nm, the TP is excited exactly at 650 nm for the TM polarization of the incident light.

Changing the metallic film thickness, we found that the maximum transmittance at the TP frequency is observed at $d_m = 50$ nm. At smaller thicknesses the reflectivity of the film is low, and at larger thicknesses the absorption is high.

The PPAM period variation leads to the change in the phase of the reflectivity φ_{PPAM}, which results in a slight shift of the TP frequency. At $2a = 600$ nm, the TP is excited for the TM polarization of the incident light at a wavelength of 648.6 nm and, at $2a = 1000$ nm, at a wavelength of 648.8 nm.

B. Chiral Optical Tamm State

If the proposed structure (Fig. 1) does not contain a metallic layer, then the COTS can still be excited at the PPAM/CLC interface. Figure 3 shows a transmittance spectrum of the PPAM/CLC structure with different CLC helix pitches and refractive indices identical of those of the PPAM, i.e., $n_e = 1.71$ and $n_o = 1.54$. The parameters correspond to the mixture of a chiral dopant (Merck, S-811) and a nematic liquid crystal (5CB). The liquid crystal is assumed to be right handed, so the light of right-handed circular polarization is reflected and the light of left-handed circular polarization is transmitted by the liquid crystal.

In the spectrum, we can see a transmission peak corresponding to the COTS. The magenta line shows the COTS position according to Eq. (10) versus CLC helix pitch p. At a helix pitch of 400 nm, the CLC and PPAM band gaps coincide; the COTS is excited exactly at 650 nm. The COTS frequency depends significantly on the angle φ between the CLC director and the optical axis of the last anisotropic layer adjacent to the CLC. Hereinafter, we restrict ourselves to the case of $\varphi = \pi/4$, where the COTS is excited exactly at the band gap center [31]. By changing the φ value, one can effectively tune the spectrum [32,33].

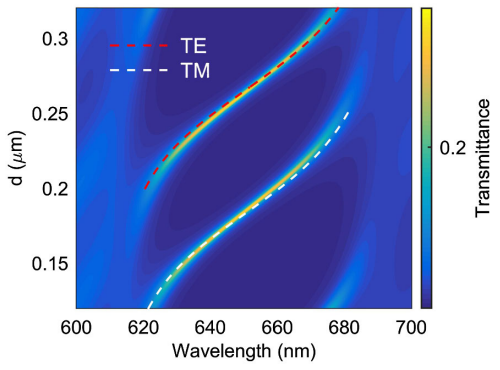

Fig. 2. Transmittance spectrum of the circularly polarized incident light for the metal–PPAM structure versus the thickness d of the layer adjacent to the metallic film. White and red lines show positions of the TP peaks for the orthogonal linear polarizations according to Eq. (6). The simulation parameters are $n_e^m = 1.71$, $n_o^m = 1.54$, $2a = 200$ nm, $N = 20$, $d_m = 50$ nm, $\epsilon_0 = 5$, $\hbar\omega_p = 9$ eV, and $\hbar\gamma = 0.02$ eV.

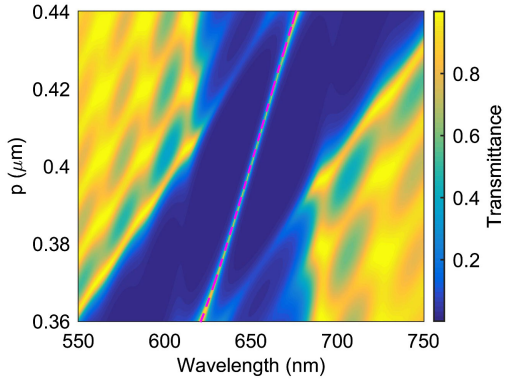

Fig. 3. Transmittance spectrum of the PPAM–CLC structure for the right-hand circularly polarized light versus CLC helix pitch p. The magenta line corresponds to the COTS frequency calculated using Eq. (10). The CLC refractive indices are $n_e = 1.71$ and $n_o = 1.54$, the thickness is 4 μm, and the parameters of the PPAM are the same as in Fig. 2.

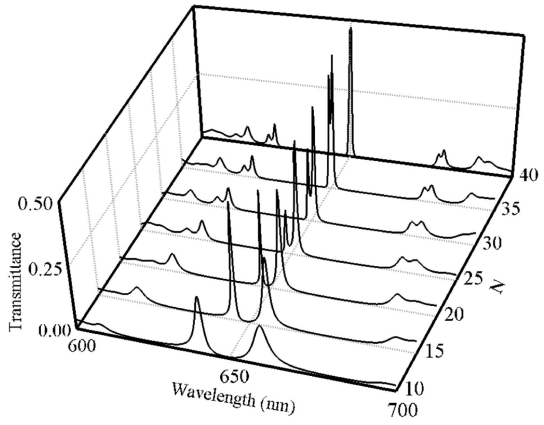

Fig. 4. Transmittance spectrum of the metal–PPAM–CLC structure shown in Fig. 1 versus the number of PPAM periods N for the right-hand circular polarization of the incident light; $p = 400$ nm, $d = 184$ nm, and the rest of the parameters are the same as in Figs. 2 and 3.

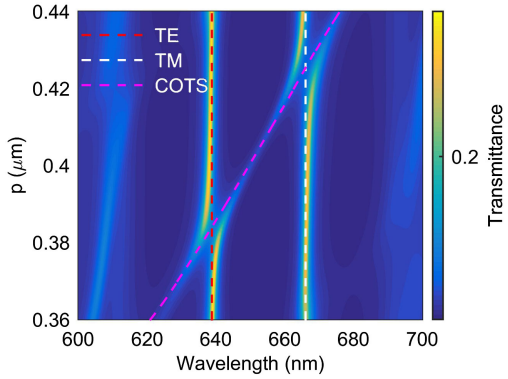

Fig. 6. Transmittance of the metal–PPAM–CLC structure shown in Fig. 1 for the right-handed circularly polarized light versus CLC helix pitch p. White and red lines show the positions of single TPs calculated using Eq. (6) for the orthogonal linear polarizations. The magenta line shows the COTS position according to Eq. (10); $p = 400$ nm, $d = 184$ nm, and the rest of the parameters are the same as in Figs. 2 and 3.

C. Hybrid Tamm Modes

When the TP and COTS frequencies in the structure shown in Fig. 1 are matched, the electromagnetic fields of localized modes overlap, which leads to the spectral splitting of the peaks. Two transmittance peaks appear in the spectrum. The splitting value depends on the PPAM thickness (Fig. 4). At $N = 40$ the field profiles' overlap is too weak to split the peaks. A decrease in the PPAM thickness led to the overlap of the Tamm modes' electromagnetic fields, which eliminated the degeneracy. The frequency split, and two transmittance peaks arose in the spectrum. At $N = 30$, the splitting value is 1 nm, $N = 20-6$ nm, and $N = 10-19$ nm.

Figure 5 shows the spatial electric field intensity distribution in the structure for wavelength of $\lambda = 641$ nm (the case of $N = 10$ in Fig. 4). The field is localized with the maxima at the interfaces. Since the light falls from the left, the field is localized stronger on the left boundary of the structure. With increasing distance to the boundaries, the fields exponentially decay. Such a field distribution confirms the excitation of hybrid modes in the structure.

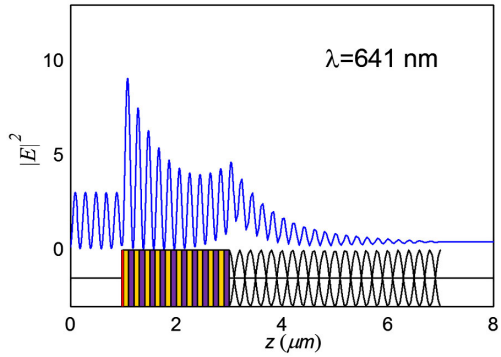

Fig. 5. Local spatial distribution of the squared electric field strength in the structure for the right-hand circular polarization of the incident light; $p = 400$ nm, $d = 184$ nm, and the rest of the parameters are the same as in Figs. 2 and 3.

An important advantage of the proposed model is the use of a CLC, which is known for its high sensitivity. Let us consider the case $d = 330$ nm. At this sublayer thickness, the TPs are excited at wavelengths of 639 and 666 nm for the TE and TM polarizations of the incident light, respectively ($N = 20$). Changing the helix pitch, we can sequentially hybridize the COTS with both TPs (Fig. 6).

The investigated model based on the hybrid TP-COTS modes can form a basis for lasers with tunable characteristics. As was shown in Ref. [37], the laser generation can be obtained using the TP arising at the interface between a multilayer mirror and a silver film. The investigated sample consisted of 40 AlAs and $Ga_{0.95}Al_{0.05}As$ periods; 15 upper periods were $Ga_{0.9}In_{0.07}As$ with quantum dots serving as an active medium. The pumping was performed through the silver layer. It was shown that, at low powers, the generation only occurs at the exciton frequency, while the growth of the latter leads to the generation at the frequency of a Tamm plasmon exciton-polariton. It was mentioned that the hybrid character of these modes paves the way to novel microlasers that can be excited electrically, with the metal film serving as an electrode. The aforementioned principle of forming an active medium is directly implementable to the suggested metal–PPAM–CLC model. It is worth noting that a feature of the structure based on the hybrid TP-COTS modes is the presence of two TP lines excited for the TE and TM waves. Thus, selecting the emission band of the quantum walls, one can ensure laser generation at two wavelengths simultaneously. The change of the CLC helix pitch (Fig. 6) is used to control the emission band splitting and obtain the two- ($450 < p > 350$) or three-mode ($350 < p < 450$) operation of the device.

Funding. Russian Foundation for Basic Research (19-52-52006).

Disclosures. The authors declare no conflicts of interest.

REFERENCES

1. A. V. Kavokin, I. A. Shelykh, and G. Malpuech, "Lossless interface modes at the boundary between two periodic dielectric structures," Phys. Rev. B **72**, 233102 (2005).
2. A. P. Vinogradov, A. V. Dorofeenko, S. G. Erokhin, M. Inoue, A. A. Lisyansky, A. M. Merzlikin, and A. B. Granovsky, "Surface state peculiarities in one-dimensional photonic crystal interfaces," Phys. Rev. B. **74**, 045128 (2006).
3. M. Kaliteevski, I. Iorsh, S. Brand, R. A. Abram, J. M. Chamberlain, A. V. Kavokin, and I. A. Shelykh, "Tamm plasmon-polaritons: possible electro-magnetic states at the interface of a metal and a dielectric Bragg mirror," Phys. Rev. B **76**, 165415 (2007).
4. C. Symonds, G. Lheureux, J. P. Hugonin, J. J. Greffet, J. Laverdant, G. Brucoli, A. Lemaitre, P. Senellart, and J. Bellessa, "Confined Tamm plasmon lasers," Nano Lett. **13**, 3179–3184 (2013).
5. A. Jimenez-Solano, J. F. Galisteo-López, H. Miguez, C. Symonds, G. Lheureux, J. P. Hugonin, J. J. Greffet, J. Laverdant, G. Brucoli, A. Lemaitre, P. Senellart, and J. Bellessa, "Flexible and adaptable light-emitting coatings for arbitrary metal surfaces based on optical Tamm mode coupling," Adv. Opt. Mater. **6**, 1700560 (2018).
6. Z.-Y. Yang, S. Ishii, S. Yokoyama, T. D. Dao, M.-G. Sun, P. S. Pankin, I. V. Timofeev, T. Nagao, and K.-P. Chen, "Narrowband wavelength selective thermal emitters by confined Tamm plasmon polaritons," ACS Photon. **4**, 2212–2219 (2017).
7. X. Wang, Y. Liang, L. Wu, J. Guo, X. Dai, and Y. Xiang, "Multi-channel perfect absorber based on a one-dimensional topological photonic crystal heterostructure with graphene," Opt. Lett. **43**, 4256–4259 (2018).
8. R. G. Bikbaev, S. Ya. Vetrov, and I. V. Timofeev, "Epsilon-near-zero absorber by Tamm plasmon polariton," Photonics **6**, 28 (2019).
9. S.-G. Huang, K.-P. Chen, and S.-C. Jeng, "Phase sensitive sensor on Tamm plasmon devices," Opt. Mater. Express **7**, 1267–1273 (2017).
10. X.-L. Zhang, J.-F. Song, X.-B. Li, J. Feng, and H.-B. Sun, "Optical Tamm states enhanced broad-band absorption of organic solar cells," Appl. Phys. Lett. **101**, 243901 (2012).
11. H. Lu, Y. Li, Z. Yue, D. Mao, and J. Zhao, "Topological insulator based Tamm plasmon polaritons," APL Photon. **4**, 040801 (2019).
12. L. Wang, W. Cai, M. Bie, X. Zhang, and J. Xu, "Zak phase and topological plasmonic Tamm states in one-dimensional plasmonic crystals," Opt. Express **26**, 28963–28975 (2018).
13. S.-C. Jeng, "Applications of Tamm plasmon-liquid crystal devices," Liq. Cryst., 1–9 (2020).
14. H. C. Cheng, C. Y. Kuo, Y. J. Hung, K. P. Chen, and S. C. Jeng, "Liquid-crystal active Tamm-plasmon devices," Phys. Rev. Appl. **9**, 064034 (2018).
15. L. Ferrier, H. S. Nguyen, C. Jamois, L. Berguiga, C. Symonds, J. Bellessa, and T. Benyattou, "Tamm plasmon photonic crystals: from bandgap engineering to defect cavity," APL Photon. **4**, 106101 (2019).
16. M. Adams, B. Cemlyn, I. Henning, M. Parker, E. Harbord, and R. Oulton, "Model for confined Tamm plasmon devices," J. Opt. Soc. Am. B **36**, 125–130 (2019).
17. M. Kaliteevski, S. Brand, R. A. Abram, I. Iorsh, A. V. Kavokin, and I. A. Shelykh, "Hybrid states of Tamm plasmons and exciton polaritons," Appl. Phys. Lett. **95**, 251108 (2009).
18. S. K. S. U. Rahman, T. Klein, S. Klembt, J. Gutowski, D. Hommel, and K. Sebald, "Observation of a hybrid state of Tamm plasmons and microcavity exciton polaritons," Sci. Rep. **6**, 34392 (2016).
19. B. I. Afinogenov, V. O. Bessonov, A. A. Nikulin, and A. A. Fedyanin, "Observation of hybrid state of Tamm and surface plasmon-polaritons in one-dimensional photonic crystals," Appl. Phys. Lett. **103**, 061112 (2013).
20. P. S. Pankin, S. Ya. Vetrov, and I. V. Timofeev, "Tunable hybrid Tamm-microcavity states," J. Opt. Soc. Am. B **34**, 2633–2639 (2017).
21. M. V. Pyatnov, S. Ya. Vetrov, and I. V. Timofeev, "Tunable hybrid optical modes in a bounded cholesteric liquid crystal with a twist defect," Phys. Rev. E **97**, 032703 (2018).
22. R. G. Bikbaev, S. Ya. Vetrov, and I. V. Timofeev, "Hybrid Tamm and surface plasmon polaritons in resonant photonic structure," J. Quant. Spectrosc. Radiat. Transfer **253**, 107156 (2020).
23. S. Kumar, P. S. Maji, and R. Das, "Tamm-plasmon resonance based temperature sensor in a TaO_5/SiO_2 based distributed Bragg reflector," Sens. Actuators A **260**, 10–15 (2017).
24. M. M. Keshavarz and A. Alighanbari, "Terahertz refractive index sensor based on Tamm plasmon-polaritons with graphene," Appl. Opt. **58**, 3604–3612 (2019).
25. O. Buchnev, A. Belosludtsev, V. Reshetnyak, D. R. Evans, and V. A. Fedotov, "Observing and controlling a Tamm plasmon at the interface with a metasurface," Nanophotonics **9**, 897–903 (2020).
26. H.-X. Da, Z.-Q. Huang, and Z. Y. Li, "Electrically controlled optical Tamm states in magnetophotonic crystal based on nematic liquid crystals," Opt. Lett. **34**, 1693–1695 (2009).
27. J. Luo, P. Xu, and L. Gao, "Controllable switching behavior of optical Tamm state based on nematic liquid crystal," Solid State Commun. **151**, 993–995 (2011).
28. V. Belyakov, *Diffraction Optics of Complex-Structured Periodic Media*, 2nd ed. (Springer, 2019), Chap. 3.1, p. 57.
29. S. Ya. Vetrov, M. V. Pyatnov, and I. V. Timofeev, "Surface modes in 'photonic cholesteric liquid crystal–phase plate–metal' structure," Opt. Lett. **39**, 2743–2746 (2014).
30. S. Ya. Vetrov, I. V. Timofeev, and V. F. Shabanov, "Localized modes in chiral photonic structures," Phys. Usp. **63**, 33–56 (2020).
31. I. V. Timofeev, P. S. Pankin, S. Ya. Vetrov, V. G. Arkhipkin, W. Lee, and V. Zyryanov, "Chiral optical Tamm states: temporal coupled-mode theory," Crystals **7**, 113 (2017).
32. N. V. Rudakova, I. V. Timofeev, R. G. Bikbaev, M. V. Pyatnov, S. Ya. Vetrov, and W. Lee, "Chiral optical Tamm states at the interface between an all-dielectric polarization-preserving anisotropic mirror and a cholesteric liquid crystal," Crystals **9**, 502 (2019).
33. M. V. Pyatnov, I. V. Timofeev, S. Ya. Vetrov, and N. V. Rudakova, "Coupled chiral optical Tamm states in cholesteric liquid crystals," Photonics **5**, 30 (2018).
34. A. Yariv and P. Yeh, *Optical Waves in Crystals* (Wiley, 1984), Chap. 6.3, p. 175.
35. M. Born and E. Wolf, *Principles of Optics: Electromagnetic Theory of Propagation, Interference and Diffraction of Light* (Pergamon, 1986), Chap. 7.6, p. 325.
36. D. W. Berreman, "Optics in stratified and anisotropic media: 4×4-matrix formulation," J. Opt. Soc. Am. **62**, 502–510 (1972).
37. C. Symonds, A. Lemaitre, P. Senellart, M. H. Jomaa, S. A. Guebrou, E. Homeyer, G. Brucoli, and J. Bellessa, "Lasing in a hybrid GaAs/silver Tamm structure," Appl. Phys. Lett. **100**, 121122 (2012).